A&A 603, A131 (2017)
DOI: 10.1051/0004-6361/201730530

Astronomy & Astrophysics

Restarting activity in the nucleus of PBC J2333.9-2343

An extreme case of jet realignment

L. Hernández-García[1], F. Panessa[1], M. Giroletti[2], G. Ghisellini[3], L. Bassani[2], N. Masetti[2,4], M. Pović[5,6], A. Bazzano[1], P. Ubertini[1], A. Malizia[2], and V. Chavushyan[7]

[1] INAF–Istituto di Astrofisica e Planetologia Spaziali di Roma (IAPS-INAF), via del Fosso del Cavaliere 100, 00133 Roma, Italy
e-mail: lorena.hernandez@iaps.inaf.it
[2] Istituto di Astrofisica Spaziale e Fisica Cosmica (IASF-INAF), via P. Gobetti 101, 40129 Bologna, Italy
[3] INAF–Osservatorio Astronomico di Brera, via E. Bianchi 46, 23807 Merate, Italy
[4] Departamento de Ciencias Físicas, Universidad Andrés Bello, Fernández Concha 700, Las Condes, Santiago, Chile
[5] Ethiopian Space Science and Technology Institute (ESSTI), Entoto Observatory and Research Center (EORC), Astronomy and Astrophysics Research Division, PO Box 33679, Addis Ababa, Ethiopia
[6] Instituto de Astrofísica de Andalucía, CSIC, Glorieta de la Astronomía, s/n, 18008 Granada, Spain
[7] Instituto Nacional de Astrofísica, Óptica y Electrónica, Apartado Postal 51-216, 72000 Puebla, Mexico

Received 30 January 2017 / Accepted 24 April 2017

ABSTRACT

Context. The giant radio galaxy PBC J2333.9-2343 shows different characteristics at different wavebands that are difficult to explain within the actual generic schemes of unification of active galactic nuclei (AGN). It is therefore a good candidate host for different phases of nuclear activity.
Aims. We aim at disentangling the nature of this AGN by using simultaneous multiwavelength data.
Methods. We obtained data in 2015 from the Very Long Baseline Array (VLBA), the San Pedro Mártir telescope, and the *XMM-Newton* observatories. This allows the study of the nuclear parts of the galaxy through its morphology and spectra and the analysis of the spectral energy distribution (SED). We also reanalysed previously-presented optical data from the San Pedro Mártir telescope from 2009 to provide a homogeneous comparison.
Results. At X-ray frequencies the source is unabsorbed. The optical spectra are of a type 1.9 AGN, both in 2009 and 2015, although showing a broader component in 2015. The VLBA radio images show an inverted spectrum with a self-absorbed, optically thick compact core ($\alpha_c = 0.40$, where $S_\nu \propto \nu^{+\alpha}$) and a steep-spectrum, optically thin jet ($\alpha_{j,8-15} = -0.5$). The SED resembles that of typical blazars and is best represented by an external Compton (EC) model with a viewing angle of approximately 3–6°. The apparent size of the large-scale structure of PBC J2333.9-2343 must correspond to an intrinsic deprojected value of approximately 7 Mpc for $\theta_v < 10°$, and to >13 Mpc for $\theta_v < 5°$, a value much larger than the biggest giant radio galaxy known, which is 4.5 Mpc.
Conclusions. The above arguments suggest that PBC J2333.9-2343 has undergone a new episode of nuclear activity and that the direction of the new jet has changed in the plane of the sky and is now pointing towards us. This changes this source from a radio galaxy to a blazar, a very exceptional case of restarting activity.

Key words. galaxies: individual: PBC J2333.9-2343 – galaxies: active – X-rays: galaxies – ultraviolet: galaxies – radio continuum: galaxies

1. Introduction

There are billions of galaxies in the Universe, all thought to host a supermassive black hole (SMBH) in their centre (e.g. Salpeter 1964; Rees 1984). Among them, some show nuclear activity and are known as active galactic nuclei (AGN). In these cases, the SMBH is fed by an accretion disc and about 10% of the AGN population show strong biconical relativistic jets (see Kellermann et al. 1989; Panessa et al. 2016, and references therein).

Nowadays, it is believed that all galaxies pass through different phases of nuclear activity. Models predict that AGN activity is a recurrent phenomenon, with all galaxies going through active states many times during their lives (Hatziminaoglou et al. 2001). It has been suggested that evolutionary processes could cause the accretion flow to vanish, giving place to a dormant nucleus. This suggestion is reinforced by the finding of massive black holes in normal galaxies (Kormendy & Richstone 1995), whereas the nuclear activity can be triggered by processes such as interaction and merging of galaxies (Bahcall et al. 1997) or by secular processes (Treister et al. 2012), which could cause the awakening of the AGN. However, the timescale of these transitions are probably too short compared to the lifetime of the galaxy, and sufficiently longer than human timescales for us to be able to observe many sources within these transitional states (e.g. Reynolds & Begelman 1997).

Nevertheless, many examples of restarted activity in the nuclei of galaxies have been reported in the literature (Saikia & Jamrozy 2009). Giant radio galaxies (GRG, Ishwara-Chandra & Saikia 1999), meaning radio galaxies with lobes of linear sizes larger than 0.7 Mpc, are perfect laboratories to study intermittent activity and galaxy evolution, because they hold huge reservoirs of energy that can have spectral ages as old as approximately 10^7–10^8 yr and can be observed even

Table 1. Observations of PBC J2333.9-2343 studied in this work.

Energy band (1)	Instrument (2)	Date (3)	Exposure (ks) (4)
X-rays/UV/Optical	*XMM-Newton* (ObsID. 0760990101)	2015-05-15	23
X-rays/UV/Optical	*XMM-Newton* (ObsID. 0760990201)	2015-11-17	25
Optical spectroscopy	San Pedro Mártir	2009-09-18	3.6
Optical spectroscopy	San Pedro Mártir	2015-11-07	5.4
Radio (8.4, 15, 24 GHz)	VLBA	2015-11-16	1.2, 2.0, 2.7

Notes. Column 1: observed energies, Col. 2: instrument or telescope, Col. 3: date, and Col. 4: exposure time.

when not fed by the jets (Alexander & Leahy 1987; Liu et al. 1992). These old lobes represent a historical record of past activity. Because the timescale for restarting activity ranges between 10^4–10^8 yr (Reynolds & Begelman 1997; Saikia et al. 2010), we can observe different phases of nuclear activity from the same nucleus in the same large-scale dataset.

Signatures of restarting activity in the jets are observed in GRGs (Saikia & Jamrozy 2009), in the form of double-double radio galaxies (DDRGs, Lara et al. 1999; Schoenmakers et al. 2000; Venturi et al. 2004; Marecki et al. 2006; Nagai et al. 2016) or as X-shaped radio galaxies (XRGs, Rottmann 2001; Gopal-Krishna et al. 2012, and references therein). Although it is not well-established as to whether the formation of DDRGs and XRGs is due to the same mechanism, it is widely accepted that the old extended radio emission is the relic of past radio activity, whereas new jet activity is the one related to smaller scale structures. Different models have been used to explain the dichotomy of these structures, such as: the double-AGN model, in which two AGN emit two pairs of jets (Lal & Rao 2007); the back-flow diversion models, in which there is a backflow from the active lobes into the wings (Leahy & Williams 1984; Kraft et al. 2005); and the jet reorientation models, which include precession or other realigning mechanisms (Rees 1978; Dennett-Thorpe et al. 2002; Merritt & Ekers 2002; Liu 2004; Gopal-Krishna et al. 2012). There are also sources in which restarted activity is deduced from indirect arguments (see e.g. Schoenmakers et al. 1998; Giovannini et al. 2007; Konar et al. 2008).

In the present work we focus on the nucleus of PBC J2333.9-2343, also named PKS 2331-240 (z = 0.0475, Parisi et al. 2012), which is located at RA = 23h33m55.2s, Dec = –23d43m41s. This AGN attracted our attention because it is a GRG (Bassani et al. 2016) that shows different and incompatible classifications when observed at different frequencies, and is therefore a good candidate to host different phases of AGN activity. Its optical spectrum is classified as a type 2 Seyfert, meaning that it presents only narrow lines and no broad components, which are typically observed in type 1 AGN (Baldwin et al. 1981; Wilkes et al. 1983; Parisi et al. 2012). Its X-ray spectrum, however, does not show signs of high obscuration, which is typically seen in Seyfert 2 (Risaliti et al. 1999; Burtscher et al. 2016). Also, Parisi et al. (2012) excluded a Compton-thick nature[1] following classical diagnostic diagrams as in Bassani et al. (1999). It seems that the source indeed behaves as a type 1 AGN at X-ray frequencies, meaning that it is unobscured. Furthermore, at radio frequencies it has many features typical of a blazar and is in fact listed in the Roma BZCAT as an object of unknown type (Massaro et al. 2009) and as a BL Lac by D'Abrusco et al. (2014) based on WISE colours; it has a flat radio spectrum (Healey et al. 2007), it shows a jet feature in a VLBI 8.4 GHz image, it is variable (Ojha et al. 2004), and it is also polarized (Ricci et al. 2004).

One explanation for the different classifications of PBC J2333.9-2343 might be attributed to variability, because the data used to classify this source were obtained on different dates. The alternative scenario is that the different classifications arise from an intrinsic property of the source. To investigate the nature of its nucleus, we perform simultaneous multiwavelength observations, including data at radio frequencies, UV, optical, and at X-rays, as well as an analysis of its simultaneous spectral energy distribution (SED).

The paper is organized as follows. Firstly, we present the multiwavelength data, and its reduction, obtained from different telescopes and satellites (Sect. 2), the results of which are reported (Sect. 3) separately for X-ray, UV, optical, and radio data, including also the analysis of the SED. We then put together the data obtained at different frequencies to discuss the possible scenario occurring in the inner parts of PBC J2333.9-2343 (Sect. 4). Finally, we summarize the main findings obtained from the present work (Sect. 5).

2. Data and reduction

In the following subsections we present the data used for the analysis and their reduction. The log of all the observations is reported in Table 1.

2.1. XMM-Newton

We used the proprietary data (PI: P. Parisi) of PBC J2333.9-2343, which was observed by *XMM-Newton* twice in 2015 only six months apart, May 15 and November 17. We used the data of the EPIC pn camera (Strüder et al. 2001). The data were reduced using the Science Analysis Software (SAS[2]), version 15.0.0. Firstly, good time intervals were selected, meaning that flares due to solar protons were excluded from the event list. The method we used for this purpose maximizes the signal-to-noise ratio (S/N) of the net source spectrum by applying a different constant-count-rate threshold to the single-event light curve with a background of $E > 10$ keV. We extracted the source, from a circular region of 25″, and background, from a circular region of 40″ free of sources and close to the nucleus, spectra with the EVSELECT task. Response matrix files (RMFs) were generated using the task RMFGEN, and the ancillary response files (ARFs) were created using the task ARFGEN. Light curves in the 0.5–10 keV, 0.5–2.0 keV, and 2.0–10.0 keV energy bands of

[1] Heavily absorbed sources with column densities greater than 1.5×10^{24} cm^{-2} (Maiolino et al. 1998).

[2] http://xmm.esa.int/sas/

the source and background were extracted using the task DMEXTRACT with a 1000 s bin.

The spectra were grouped using the GRPPHA task to have a minimum of twenty counts per bin. This allows the use of χ^2-statistics. It is worth noting that the pileup fraction is negligible, below 1% as estimated with PIMMS[3] using a power-law model.

Data from the Optical Monitor (OM, Mason et al. 2001) onboard *XMM-Newton* are available in the UVW1 (centred at 2675 Å), U (centred at 3275 Å), and V (centred at 5468 Å) filters in the two dates. The aperture photometry was performed by using the processing chain OMICHAIN to select circular regions of 5″ centred on the source and of 20″ for background regions.

2.2. San Pedro Mártir telescope

The nucleus of the galaxy LEDA 71756, the optical counterpart of PBC J2333.9−2343, was observed on September 18, 2009, and on November 7, 2015 with the 2.12 m telescope of the San Pedro Mártir Observatory (México), equipped with a Boller & Chivens spectrograph and a 650 × 2048 pixels E2V-4240 CCD. In this section we report only the data reduction for the spectrum obtained in 2015, because the spectrum from 2009 was reduced and published in Parisi et al. (2012) and we refer the reader to that paper for more details on the data reduction. However, in this work a stellar population subtraction was applied for the first time to both spectra (see details in Sect. 3.2).

Three 1800s spectra with a dispersion of approximately 2.3 Å/pix were acquired starting at 03:15 UT on November 7, 2015; they nominally covered the 3600–8200 Å wavelength range. The spectra were acquired on the galaxy nucleus with a slit aperture of 2.5 arcsec. Data reduction was carried out using standard procedures for both bias subtraction and flat-field correction with the image reduction and analysis facility (IRAF[4]).

The wavelength calibration was carried out with neon-helium-copper-argon lamps; the uncertainty was approximately 0.5 Å according to the position of the background night sky lines. The flux calibration was performed using the catalogued spectroscopic standard star G191−B2B (Massey et al. 1988). The three spectra were then stacked together to obtain one final spectrum with the best possible S/N.

It is worth noting that the values of the airmass during the observations was high, 1.7–1.8, and consequently the separation between blue and red wavelengths is large; thus the spectroscopic flux measurements need to be taken with caution. However, the estimates on line widths and ratios are reliable, providing a robust classification of the source.

2.3. Very long baseline array (VLBA)

We observed the nucleus with the NRAO[5] Very Long Baseline Array (VLBA) on 2015 November 16. We observed for two hours at 8.4, 15, and 24 GHz, with a net on source time of 20, 33, and 45 m at each frequency, respectively. Ice and cold weather affected the focus or rotation mount at Mauna Kea, so that data were obtained from that station only for a limited part of the observations. No other complications were reported.

The observing frequency band was divided in 16 × 32 MHz baseband channels, in dual polarization, for a total recording rate of 2 Gbps. We carried out a standard calibration using the astronomical image processing system (AIPS), following the new prescription for amplitude calibration described by Walker (2015). We removed single-band delays with pulse-cal table information, and the residual delays and phase rates by fringe fitting the target source itself. We then averaged the frequency channels and produced the final images in Difmap, with several cycles of phase-only and phase-and-amplitude self-calibration, with solution intervals of decreasing length. The noise levels are within a factor of two of the predicted thermal values, which is reasonable given the non-ideal coverage of the (u, v)-plane for short observations of a low declination source, and the somewhat complex structure of the object.

3. Data analysis and results

3.1. X-ray spectroscopy and UV and optical photometry

Firstly, we checked whether X-ray variations are observed on short timescales, meaning intra-day variability. We analyzed the *XMM-Newton* light curves in three energy bands, the soft (0.5–2 keV), hard (2–10 keV), and total (0.5–10 keV). We calculated the normalized excess variance, $\sigma^2_{\rm NXS}$, following prescriptions in Vaughan et al. (2003; see also González-Martín & Vaughan 2012). None of the light curves showed short-term variations, meaning that all are compatible with zero within the errors.

We then performed the spectral analysis using XSPEC v. 12.9.0. We assumed a redshift of $z = 0.0475$ (Parisi et al. 2012) and a Galactic absorption of $N_{\rm Gal} = 1.63 \times 10^{20}$ cm^{-2} as obtained within FTOOLS (Dickey & Lockman 1990; Kalberla et al. 2005). Different models were tested to select the simplest one which fitted the X-ray data well. Firstly, these models were fitted to each spectrum individually. Initially, we fitted a single power law representing the AGN continuum. This model represented the data well, but we nonetheless checked whether there was an improvement of the fit when different components were added. We added neutral absorption using a ZWABS component, then changed the absorption by a partial covering component (PCFABS in XSPEC), added a thermal component (MEKAL in XSPEC) or another power law, and also fitted these components absorbed by an intrinsic column density. The χ^2/d.o.f $= \chi^2_{\rm r}$ and *F-test* were used to select the best-fitting model, considering an improvement on the spectral fit when χ^2/d.o.f is as closest as possible to the unity and the *F-test* results in a value larger than 10^{-5}. None of these components improved the fits, thus the best representation of the data is obtained by a single power-law model. The results of the spectral parameters and X-ray fluxes and luminosities are reported in Table 2, marked as Individual in Col. 1. The individual spectral fits agree well with those reported by Parisi et al. (2012) for *Swift* data.

As a second step, we fitted the two *XMM-Newton* spectra simultaneously. This process allows us to search for X-ray spectral variability (Hernández-García et al. 2013). We found that linking all the parameters to each other did not result in a good spectral fit, χ^2/d.o.f. = 1865.9/1291.

We therefore let the spectral index, Γ, and the normalization of the power law, *Norm*, vary in the model one-by-one. The model in which *Norm* varied showed an improvement, such that *F-test* $= 1 \times 10^{-100}$, whereas varying Γ did not show an improvement of the fit. We also let the two spectral parameters vary together, meaning Γ + *Norm*, but no improvement of the spectral fit was detected.

Thus, our results show that PBC J2333.9-2343 has undergone a small luminosity decrease, 16%, of its nuclear power

[3] http://cxc.harvard.edu/toolkit/pimms.jsp
[4] http://iraf.noao.edu/
[5] The National Radio Astronomy Observatory is a facility of the National Science Foundation operated under cooperative agreement by Associated Universities, Inc.

Table 2. Spectral parameters of the X-ray spectra of PBC J2333.9-2343 obtained by *XMM-Newton* using a power-law model and UV and optical photometry from the OM.

Analysis	ObsID	Γ	Norm	Flux (2–10 keV)	L(2–10 keV)	χ^2_r	$UVW1$	U	V
			($\times10^{-3}$)	($\times10^{-11}$ erg s^{-1} cm^{-2})	($\times10^{43}$ erg s^{-1})		($\times10^{-16}$ erg s^{-1} cm^{-2})		
(1)	(2)	(3)	(4)	(5)	(6)	(7)	(8)	(9)	(10)
Individual	0760990101	$1.77^{1.78}_{1.75}$	$2.61^{2.64}_{2.59}$	$0.96^{0.98}_{0.95}$	$5.07^{5.16}_{4.98}$	1.03	8.41 ± 0.13	7.01 ± 0.09	18.78 ± 0.19
	0760990201	$1.77^{1.79}_{1.76}$	$2.18^{2.20}_{2.15}$	$0.79^{0.81}_{0.77}$	$4.16^{4.27}_{4.07}$	0.99	8.55 ± 0.12	6.70 ± 0.07	19.55 ± 0.14
Simultaneous	0760990101	$1.77^{1.80}_{1.76}$	$2.67^{2.71}_{2.63}$	$0.97^{0.99}_{0.93}$	$5.06^{5.16}_{4.96}$	1.02			
	0760990201		$2.23^{2.26}_{2.19}$	$0.78^{0.80}_{0.75}$	$4.23^{4.29}_{4.19}$				

Notes. Column 1: type of analysis, where individual means that each spectrum was analyzed, and simultaneous means that the two spectra are analyzed together (we note that the normalization of the power law is variable, therefore each of the lines correspond to the values of the spectral parameters of the observations in Col. 2), Col. 2: ObsID., Col. 3: spectral index, Col. 4: normalization of the power law, Cols. 5 and 6: X-ray intrinsic flux and luminosity in the 2–10 keV energy band, Col. 7: reduced χ^2, and Cols. 8–10: fluxes from the OM in units of 10^{-16} erg cm^{-2} s^{-1}. In all cases $z = 0.0475$ and $N_G = 1.63 \times 10^{20}$ cm^{-2}. The errors are indicated as interval limits and are estimated at the 90% confidence.

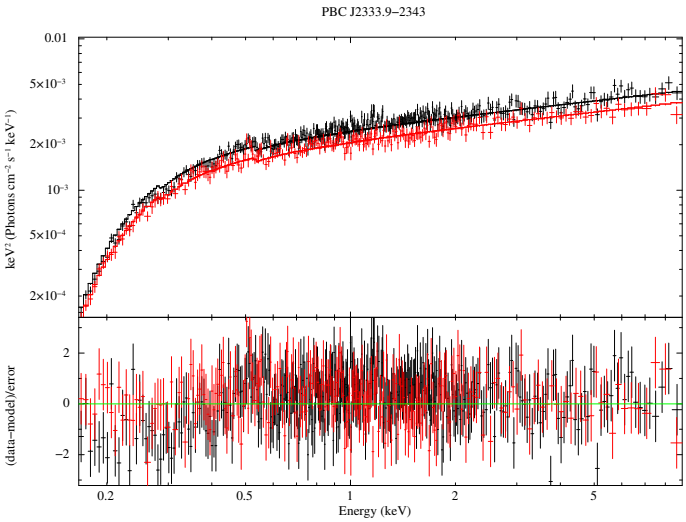

Fig. 1. Simultaneous spectral fitting of the *XMM-Newton* spectra of PBC J2333.9-2343 using a single power-law model. The black spectrum corresponds to ObsID. 0760990101 and the red spectrum corresponds to ObsID. 0760990201.

during the timescale of six months. PBC J2333.9-2343 has an intrinsic column density compatible with the Galactic one, for which we estimated an upper limit of $N_H < 2.7 \times 10^{20}$ cm^{-2} on the intrinsic absorption, a spectral slope of about 1.8, and a variable normalization of the power law. In Fig. 1 we present the simultaneous spectral fit for *XMM-Newton* data when varying *Norm*. The results of the spectral fit can be found in Table 2, marked as Simultaneous in Col. 1. It is worth noting the presence of residuals in the 0.5–1 keV energy range that might be due to emission or absorption features. We added Gaussian components to represent these lines in the spectral fitting but, using C-statistics, none of them were significant for the spectral fit. We also checked the data from the reflection grating spectrometer (RGS), which show hints of spectral lines, but a longer observation is needed to reproduce these spectral features.

Finally, we obtained the UV and optical photometry from the OM in three filters: UVW1, U, and V, the measurements of which are presented in the right-hand part of Table 2. Variations between the two dates, which were separated by six months, that were observed by OM were not detected in the UVW1 filter, because the fluxes are compatible within the errors. A small variation of 4% was detected both in the optical U and V filters.

3.2. Optical spectroscopy

We estimated the stellar population using the STARLIGHT V.04 stellar population synthesis code (Cid Fernandes et al. 2005, 2009) for the spectra obtained in 2009 and 2015. This code decomposes an observed spectrum in terms of a superposition of a base of simple stellar populations of various ages and metallicities, outputting physical properties as, for example, the star-formation and chemical-enrichment histories of a galaxy. Before the subtraction of the stellar population, the spectra were corrected for Galactic extinction, K-corrected, and moved to rest frame. We used the fits based on the templates from Bruzual & Charlot (2003), with solar metallicity, and twenty five stellar ages in the range 1×10^6–1.8×10^{10} yr, and the extinction law of Cardelli et al. (1989). During the fitting process, all the areas with emission lines, noise, and atmospheric absorption were masked. It is worth noting that both spectra were affected by detector fringing above 7000 Å, and thus they were cut after the [S II] line at about that wavelength. Finally, the 3600–7000 Å wavelength range was used for the analysis. We caution that the CCD sensitivity in the blue region of the 2009 spectrum is low, resulting in strong residuals in the 4000–4800 Å wavelength range when performing the stellar population subtraction because it cannot be well-fitted with STARLIGHT. The spectra subtracted by the stellar population from the STARLIGHT fits are presented in Fig. 2.

The main properties of the optical spectra are presented in Table 3. The S/N was obtained directly from the best-fitted models. To measure the current ($M_\star$) and initial ($M_\star(initial)$) mass in stars, star formation rate (SFR), and mean age (log(Āge)), we followed the same procedures as in Pović et al. (2016, and references therein). The independent measurements of $M_\star$, $M_\star(initial)$, log(Age), and SFR as listed in Table 3 agree well within the errors. Line fluxes were obtained by means of the splot IRAF task by fitting a single Gaussian function and the errors were measured taking into account the rms of the continuum. The resulting best-fitted models show that both spectra are completely dominated by old stellar populations with ages $>10^9$ yr.

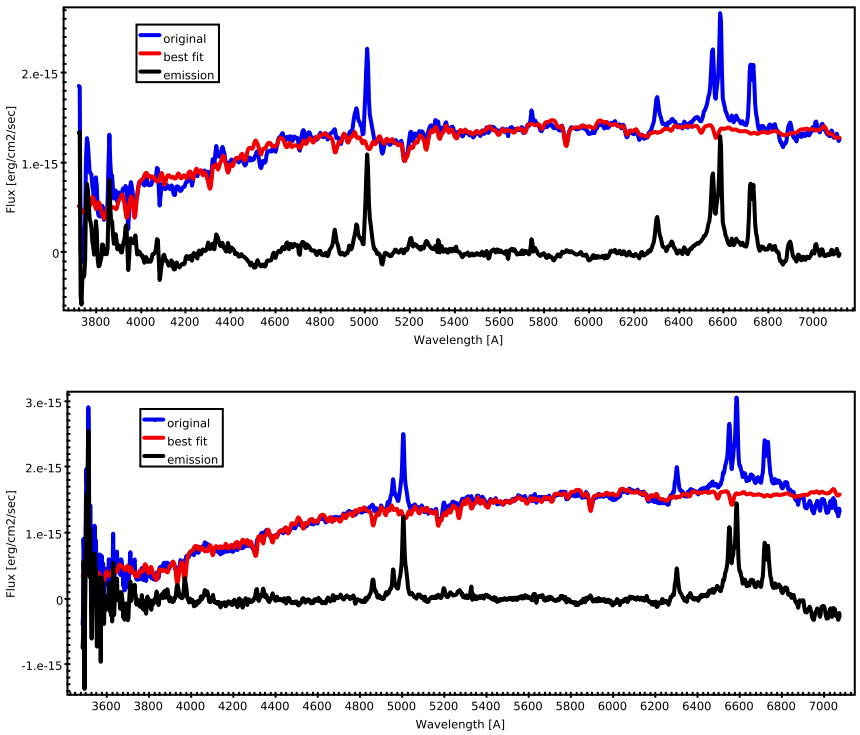

Fig. 2. Optical spectra of PBC J2333.9-2343 obtained with the San Pedro Mártir Observatory in 2009 (*up*) and 2015 (*bottom*). The blue corresponds to the original spectrum, the red to the best-fitted model, and the black to the stellar population subtracted spectrum (i.e. observed – best-fitted model).

Table 3. Main properties of the optical spectra (see Fig. 2).

Property	2009	2015
(1)	(2)	(3)
S/N	54.6 ± 1.1	57.1 ± 1.1
$\log M_\star$	10.77 ± 0.18	10.61 ± 0.19
$\log M_\star(initial)$	11.07 ± 0.22	10.87 ± 0.23
log(Āge)	9.78 ± 0.12	9.52 ± 0.12
SFR	6.55 ± 1.44	4.16 ± 0.91
Flux(H_β)	5.61 ± 0.67	5.56 ± 1.13
Flux([O_{III}(4959)])	5.52 ± 1.02	8.23 ± 1.13
Flux([O_{III}(5007)])	19.23 ± 1.02	22.10 ± 1.13
Flux([O_I(6300)])	9.98 ± 1.14	9.30 ± 0.85
Flux([N_{II}(6548)])	13.10 ± 9.73	13.49 ± 1.01
Flux(H_α)	3.12 ± 0.97	5.66 ± 1.01
Flux([N_{II}(6584)])	19.37 ± 0.97	20.00 ± 1.01
Flux([S_{II}(6717)])	11.15 ± 0.88	8.00 ± 0.58
Flux([S_{II}(6731)])	8.87 ± 0.88	7.47 ± 0.58

Notes. Column 1: property, where all the fluxes are measured in units of 10^{-15} erg s^{-1} cm^{-2}, Col. 2: value for the spectrum taken in 2009, and Col. 3: value for the spectrum taken in 2015. For more information about flux measurements and their reliability see Sect. 2.2.

The optical spectrum of PBC J2333.9−42343 obtained in 2015 does not differ substantially from the one obtained in 2009, which was first presented in Parisi et al. (2012), without the stellar population subtraction. Indeed, the line fluxes of the emission lines are similar between the two spectra, as is the continuum level (see Table 3)[6]. We also remark that source continuum and narrow emission lines do not show significant variability among the spectra acquired in the framework of the present paper.

Nevertheless, one peculiarity is found when comparing our results with those reported in Parisi et al. (2012). In their paper, the authors classified this source as a type 2 Seyfert. In the present analysis, using the same spectrum from 2009 and thanks to the subtraction of the stellar population, we report the existence of a broad component at the foot of the H_α+[NII] complex. However, we are not able to measure it in the observation from 2009 because it is very weak. Recent spectra taken in 2016 confirm the current presence of the broad H_α line and will be presented in a forthcoming paper (Hernández-García et al., in prep.).

The broad component in the H_α+[NII] complex is more marked in the 2015 spectrum, which has a full width at half maximum (FWHM) of about 370 Å, corresponding to a velocity of approximately 16700 km s^{-1}, and a flux of 1.6 × 10^{-13} erg cm^{-2} s^{-1} (although see Sect. 2.2). This might suggest a small amount of variability in the broad line region (BLR) between the two dates, although we cannot quantify it. Therefore, because a broad component was found in H_α both in 2009 and 2015, but not in H_β, we suggest that this source is a type 1.9 AGN according to the classification criteria given by Osterbrock (1981).

We also note that the optical spectra show some evidence of a "blue wing" affecting all nebular lines, which may trace an ionized outflow. A detailed analysis of this outflow component will be presented in a forthcoming paper (Hernández-García et al., in prep.).

Finally, we can estimate the black hole mass, M_{BH}, using the relation in Greene & Ho (2005), which relates the FWHM(H_α) and the flux of the H_α broad component[7] with M_{BH}. From this approach and using the data from 2015, we obtain M_{BH} = 5.7 ± 2.3 × 10^8 $M_\odot$. Alternatively, we can estimate the M_{BH} from the velocity dispersion derived with STARLIGHT. Assuming an average instrumental resolution, from the FWHM

[6] It is worth noting here that the measurements of H_α, [NII], and [SII] might be affected by the broad component and thus they cannot be completely reliable.

[7] We note that the measurement of the flux has to be taken with caution (see Sect. 2.2).

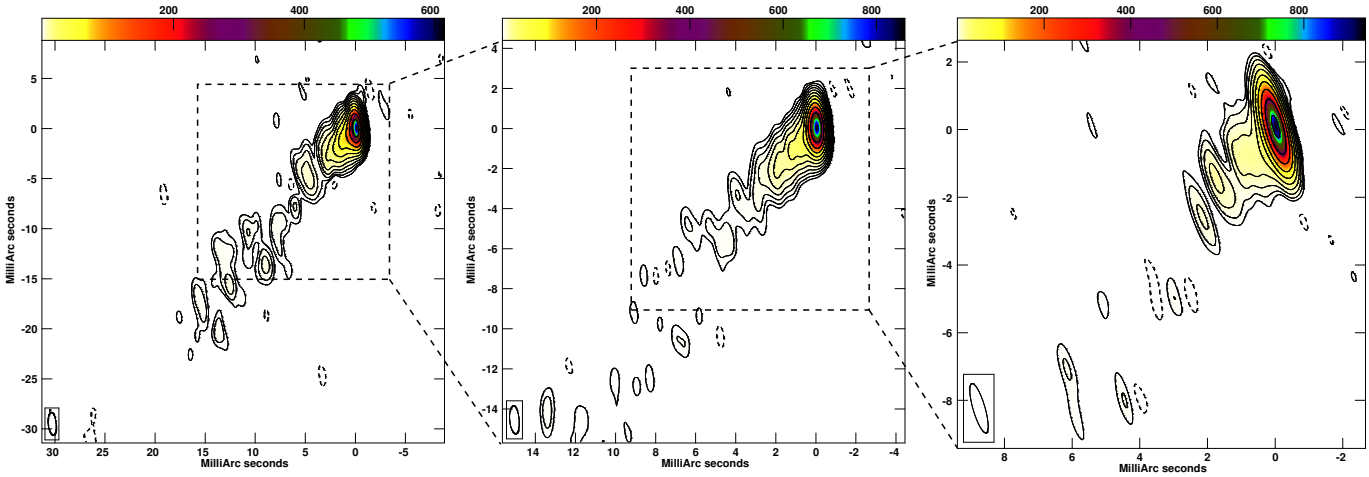

Fig. 3. VLBA images of PBC J2333.9-2343 at 8, 15, and 24 GHz (*left to right*). Contours are traced at $(-1, 1, 2, 4, \ldots) \times 0.4$, 0.4, 1.6 mJy beam^{-1} in each image, respectively. The restoring beam is shown in the bottom left corner of each panel and its value is given in Table 4. The dashed box in *the left panel* indicates the region displayed in the middle one; the one in *the middle panel* indicates that of the right hand side one. The colour scale range shows surface brightness in mJy beam^{-1} between 0 (yellow) and the image maximum (blue), as shown in the top wedge of each panel.

Table 4. VLBA image parameters.

ν (GHz) (1)	Duration (m) (2)	*HPBW* (mas × mas, °) (3)	σ_ν (mJy beam^{-1}) (4)	I_ν (mJy beam^{-1}) (5)	S_ν (Jy) (6)
8	25	$2.3 \times 0.8, 5.4$	0.08	610	0.91
15	33	$1.4 \times 0.5, 4.7$	0.08	810	1.16
24	45	$1.5 \times 0.35, 16.3$	0.34	940	1.23

Notes. Column 1: frequency, Col. 2: duration, Col. 3: half peak beam width (HPBW), Col. 4: image noise, Col. 5: image peak brightness, Col. 6: total cleaned flux density.

of the sky lines, of 9 Å in the range between 4000–7000 Å, meaning a central wavelength of 5500 Å), this yields a corrected velocity dispersion of 330 km s^{-1}. Using the M-σ relation in Gültekin et al. (2009) we estimate a black hole mass of $M_{\rm BH} = 5.6 \pm 1.3 \times 10^8\ M_\odot$.

3.3. Radio

The source is well-detected at all three frequencies of 8, 15, and 24 GHz; see Table 4 for details on the image parameters at each frequency. It is characterized by a compact bright core and a jet (see Fig. 3). The overall source flux is fairly similar at the various frequencies, indicating a flat radio spectrum. In Fig. 4, we show the spectral index image between 8 and 15 GHz, obtained from images produced using the same baseline length range, 8–240 Mλ, and restoring beam, which was circular with a half-power beam width (HPBW) of 2.3 mas. The spectral index α is defined such that $S(\nu) \approx \nu^{+\alpha}$.

The core is the main feature in the VLBA images. Its peak brightness varies between 610 and 940 mJy beam^{-1}, increasing with frequency. The mean spectral index is $\alpha_{\rm c} = 0.40 \pm 0.04$ based on a linear fit to these values, which is in agreement with that shown by the spectral index image (Fig. 4). This behaviour indicates that the core region is in an optically thick regime. The brightness temperature is about 10^{12} K, providing a first indication that the Doppler factor $\delta = [\Gamma(1 - \beta \cos\theta_v)]^{-1}$ is greater than unity; with standard notation, $\Gamma = (1 - \beta^2)^{-1/2}$, $\beta = v/c$, in which v is the jet velocity and θ is the jet viewing angle.

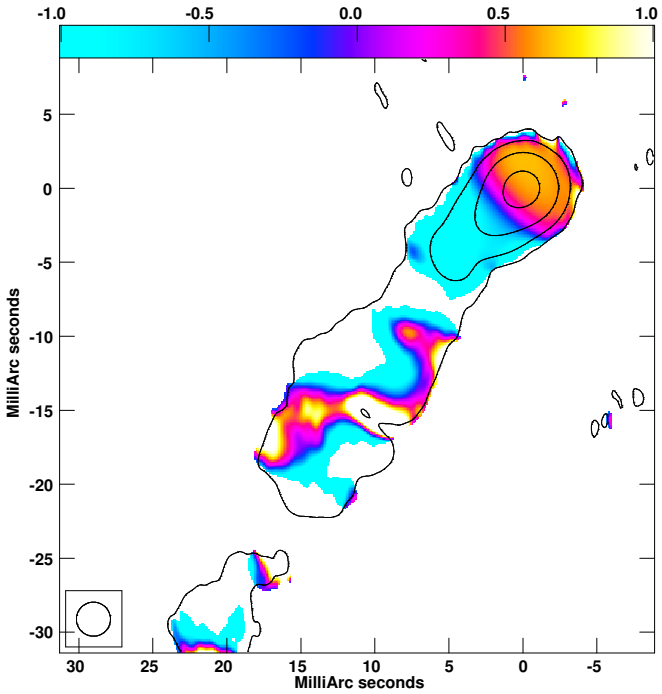

Fig. 4. VLBA spectral index image of PBC J2333.9-2343 between 8 and 15 GHz, overlaid with 8 GHz total intensity contours. The colour scale range is $-1 < \alpha < +1$ and it is shown by the wedge on the top; contours are traced at $(1, 10, 100, 1000) \times 0.35$ mJy beam^{-1}.

The core is at the base of a one-sided jet that extends in position angle $\varphi = 133°$. The jet is brighter at 8 GHz, where it extends out to over 60 mas, ~53 pc, as best seen in naturally weighted images. The brighter jet at 8 GHz is in agreement with optically thin synchrotron emission, as also indicated by the steep values of the spectral index seen in Fig. 4; the average value in the jet region is $\alpha_{j,8-15} = -0.5$.

The large-scale structure of PBC J2333.9-2343 is two-sided, indicating that asymmetries on parsec scales are most likely the result of Doppler beaming. We set a lower limit to the jet/counter-jet brightness ratio R using the jet brightness at approximately one beam from the core and the 1σ rms noise level on the counter-jet side; in particular, for the 8 GHz image, we get $R > 10^3$. In turn, by using the observed spectral index value of α_j, we get $\beta \cos\theta_v > 0.76$. Interestingly, this immediately implies that $\theta_v < 40°$. The comparison of the jet position angle (PA) on parsec and kiloparsec scales does not suggest the presence of strong viewing angle changes; indeed, Graham & Tingay (2014) report a jet PA of $\varphi = 139°$ and a lack of PA changes in the parsec scale of PBC J2333.9-2343, based on the images in Fomalont et al. (2000), Ojha et al. (2004), and in the radio fundamental catalogue (RFC, version rfc2013d).

Finally, we can compare our image at 8 GHz with those at the same frequency reported by Ojha et al. (2004) and in the RFC. We find flux density variability, with the source being approximately 300 mJy brighter in the present epoch. The jet PA has not changed significantly in comparison to the RFC; also the difference to the PA reported by Ojha et al. (2004, $\varphi = 121°$), is not highly significant, in particular if we consider that the array used by these authors had a very limited coverage of the (u, v)-plane. The time separation between the three datasets is more than 11 yr, making the component identification highly uncertain. At the redshift of the source, an apparent proper motion with velocity $\beta = 1$ would correspond over this time range to a displacement of approximately 4.2 mas. This means that, if they are travelling with $\beta = 1$, all the components present in the archival data have now moved to the region where the jet is transversally resolved and the compact components have been disrupted.

3.4. Spectral energy distribution (SED)

The analysis of the spectral energy distribution (SED) was carried out using the simultaneous data presented in this work. The strong and flat radio emission, the large radio–loudness, and the strong X-ray emission all suggest that the flux produced by the jet is a very important component for modelling the entire SED, which resembles closely the SED of typical blazars (Ghisellini & Tavecchio 2015).

With the aim of reproducing the overall SED, we used the model fully described in Ghisellini & Tavecchio (2009). It is a one–zone leptonic model that assumes that the emitting region is a sphere of radius $R = \psi R_{\rm diss}$, where $R_{\rm diss}$ is the distance from the black hole, and ψ is the jet opening angle, assumed to be conical. The source is moving at a relativistic velocity β_c corresponding to the bulk Lorentz factor Γ. This region is observed at a viewing angle θ_v, so that the relativistic Doppler factor is $\delta \equiv 1/[\Gamma(1 - \beta \cos\theta_v]$.

The energy distribution of the emitting particles is derived by solving a continuity equation assuming that particles are uniformly injected throughout the source, and considering radiative cooling, electron–positron pair production, and the contribution of these pairs to the observed flux. The considered emission processes are synchrotron, synchrotron self–Compton (SSC), and inverse Compton scattering off photons produced externally to the jet (EC), by the disc, by the BLR and by the molecular torus.

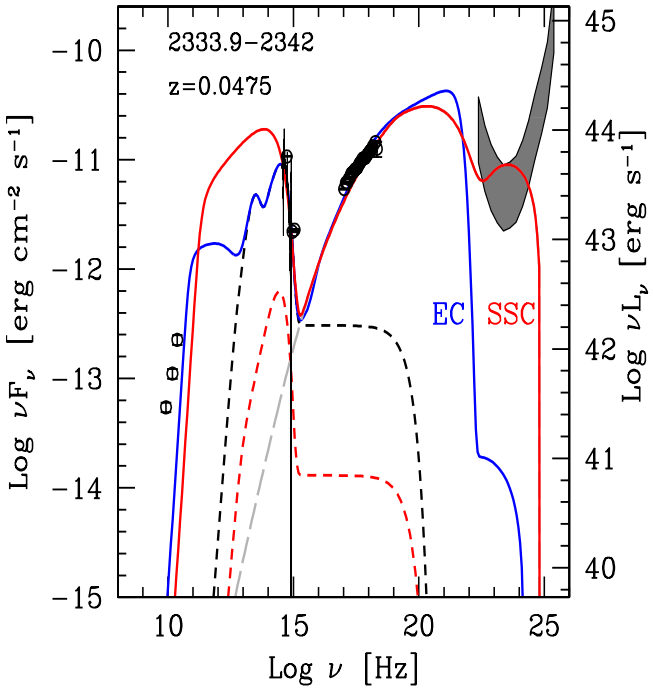

Fig. 5. The SED of PBC J2333.9–02343 using simultaneous data from the VLBA and *XMM-Newton* observatories. The grey stripe corresponds to the 5σ sensitivity of *Fermi*/LAT after 1 yr (top margin) and 5 yr (bottom margin) of observations. The solid lines refer to the theoretical models: for the continuous red line it is assumed that the seed photons used for the Inverse Compton scattering are the synchrotron ones produced by the same electrons (SSC); for the continuous blue line the process is External Compton (EC) with seed photons produced by the torus. The black dashed line represents the disc; the red dashed line represents the corona.

The emitting source is compact, as in other blazars. In our case, $R_{\rm diss} = 300$–400 Schwarzschild radii. This kind of a compact region produces a synchrotron spectrum that is self–absorbed below approximately 100 GHz, and therefore cannot account for the radio flux at smaller frequencies. This has to be produced by other, more extended, portions of the jet.

Figure 5 shows the overall SED of PBC J2333.9-2343 together with our models. The grey area represents the 5σ sensitivity of *Fermi*/LAT after 1 yr (top margin) and 5 yr (bottom margin) of observations. Table 5 lists the parameters used for the EC and SSC models. We recall that details on the models and on how to estimate the parameters can be found in Ghisellini & Tavecchio (2009).

We have searched in the Fermi archive[8] for indications of γ-ray emission from the source but did not detect any, as reported also by Giommi et al. (2012). Using the Fermi LAT photon event and spacecraft data query and online data analysis tool[9], we find that PBC J2333.9-2343 is not close to the Galactic plane nor to a blazar, thus the non-detection cannot be related to these problems. Moreover, we estimate the Fermi upper limit for this source, which lies within the grey area in Fig. 5. Because the detection of this source is expected under the SSC scenario, we suggest that the preferred main emission process in PBC J2333.9-2343 is EC.

[8] http://fermi.gsfc.nasa.gov/ssc/
[9] http://tools.asdc.asi.it/?&searchtype=fermi

Table 5. Adopted parameters for the jet models.

	M	$L_{\rm d}$	$L_{\rm d}/L_{\rm Edd}$	$R_{\rm diss}$	$R_{\rm BLR}$	$R_{\rm torus}$	$P'_{\rm e,jet,45}$	B	Γ	θ_v
(1)	(2)	(3)	(4)	(5)	(6)	(7)	(8)	(9)	(10)	(11)
EC	3.0e9	0.047	1.3e–4	360	22	540	1e–3	0.14	10	3
SSC	–	–	–	90	–	–	7e–3	0.17	13	6

Notes. Column 1: model type, Col. 2: black hole mass in solar masses, Col. 3: disc luminosity in units of 10^{45} erg s^{-1}, Col. 4: disc luminosity in units of the Eddington luminosity, Col. 5: distance of the dissipation region from the black hole, in units of 10^{15} cm, Col. 6: size of the BLR, in units of 10^{15} cm, Col. 7: size of the torus, in units of 10^{15} cm, Col. 8: power injected in the jet in relativistic electrons, calculated in the comoving frame, in units of 10^{45} erg s^{-1}, Col. 9: magnetic field in G, Col. 10: bulk Lorentz factor, Col. 11: viewing angle in degrees.

From the EC model, and assuming a standard accretion disc (Shakura & Sunyaev 1973), we estimate a $M_{\rm BH} = 3 \times 10^9 M_\odot$ from the frequency of the peak of the accretion disc spectrum and its flux. However, the peak is not well-determined, therefore the uncertainty is about a factor of two. It is worth noting that this value is roughly consistent with that obtained from the optical data (see Sect. 3.2), taking into account that both measurements are not accurate. The accretion disc emits a luminosity $L_{\rm d} \sim 5 \times 10^{43}$ erg s^{-1}, therefore the Eddington ratio is $R_{\rm Edd} = L_{\rm d}/L_{\rm Edd} \sim 1.3 \times 10^{-4}$. For the modelling, we used a standard disc spectrum (Shakura & Sunyaev 1973), even if the Eddington ratio indicated that theoretically we are likely in the advection dominated accretion flow (ADAF, Narayan & Yi 1994) regime. In any case, the seed photons that we use for the inverse Compton process are produced by the torus, not by the BLR clouds. If the disc is emitting the same luminosity, but in ADAF mode, we would have a different optical–UV spectrum. However, the energy density of the radiation produced by the torus would remain unchanged, because the torus reprocesses all the incoming radiation largely independently from its spectrum.

Given our aim, the most important and robust result is that the observed level of radio emission and X-ray flux and slope can be reproduced only if the jet is observed at small, 3–6° viewing angles. At larger angles the SED cannot be well-reproduced. In particular, the Doppler factor, hence the flux enhancement, decreases sufficiently to require impossibly large intrinsic, meaning comoving, luminosity to account for the observed data. In addition, larger angles imply an increasing importance of the second order Compton scattering, which contributes in the gamma-ray band with a flux that should become visible by Fermi/LAT. Nevertheless, high-energy data (*Swift*/BAT, *NuSTAR*, INTEGRAL, *Fermi*) would be useful to better constrain our model parameters, in particular θ_v.

4. Discussion

The classification of the nucleus of PBC J2333.9-2343 has been controversial in the literature, being classified as a Seyfert 2 in the optical, as unobscured AGN at X-rays, and as a blazar at radio frequencies (see Parisi et al. 2012). Because these classifications were obtained using data at different epochs, we obtained simultaneous coverage at X-ray, UV, optical, and radio frequencies, and find that these conflicting classifications cannot be related to variability complications[10]; instead they have to be attributed to an intrinsic property of the nucleus. Our observational results show that, in this source, both the jet and the nucleus are visible, with the jet closely pointing towards us, but we still have a direct view onto the BLR. This suggests that PBC J2333.9-2343 is a blazar, explaining well all the classifications given at different wavebands.

The SED and radio analysis of this source suggest that the jet is observed at small angles. This line of sight is in good agreement with the lack of $N_{\rm H}$ inferred from the analysis of the X-ray data, which indicates that the source emission is not absorbed, as well as with the presence of a broad component in the optical spectrum, which suggests that the BLR is at least partly observed. For this small θ_v, and using public data from the NRAO VLA Sky Survey (NVSS, Condon et al. 1998), the apparent size of the large-scale structure of PBC J2333.9-2343, at approximately 22′ or approximately 1150 kpc as per the left panel in Fig. 6, must correspond to an intrinsic deprojected value of approximately 7 Mpc for $\theta_v < 10°$, and to >13 Mpc for $\theta_v < 5°$, as suggested by the SED results. The projected linear size of the largest giant radio galaxy known up to now is 4.69 Mpc (Machalski et al. 2008). Moreover, Andernach et al. (2015) used a sample of 193 radio galaxies and determined that only one is a candidate to have a size larger than 5 Mpc. Thus, although it is highly implausible that the size of this source is so large, we leave this possibility open. Alternatively, this result might indicate that the direction of the jet has changed. This behaviour has been reported in the literature before, with changes in the direction of the jet as large as approximately 90° (Giovannini et al. 2005), and towards smaller angles too (Evans et al. 1999; Saripalli et al. 2002; Konar et al. 2006; Saikia & Jamrozy 2009; Gopal-Krishna et al. 2012; Marecki 2012; Saripalli et al. 2013). The case of PBC J2333.9-2343 is exceptional, because the realignment of the jet changed this galaxy from a radio galaxy to a blazar. Moreover, if we compare the PA of the jets in the VLA and VLBA data, with values of 139° and 133°, respectively, it seems that this change has occurred in a direction that, by chance, conserved the projected PA.

A change in the direction of the jet could be ascribed to restarting activity in the nuclei of the galaxies, meaning when the nuclear activity at some point decreases or stops and then it restarts (Christiansen 1973). Observational indications of restarting activity can be inferred in radio galaxies from their extended emission. The old lobes can survive up to approximately 10^7–10^8 yr and trace the largest scale emission from the nucleus (Konar et al. 2006), whereas the new activity can be observed at smaller scales. The result is that the different phases of activity can be observed in the same image. The analysis of the stellar populations shows that PBC J2333.9-2343 is composed by stars on average older than 10^9 yr, therefore the galaxy has had enough time to form the old lobes and be subject to recurrent activity episodes.

The most striking evidence of restarting activity is given by the unambiguous morphology of DDRG and XRG. Although we do not see indications of such morphologies in our data, the fact that the jet reorientation made this source to become

[10] We note that the only difference is that we classified it as a type 1.9 AGN in the optical.

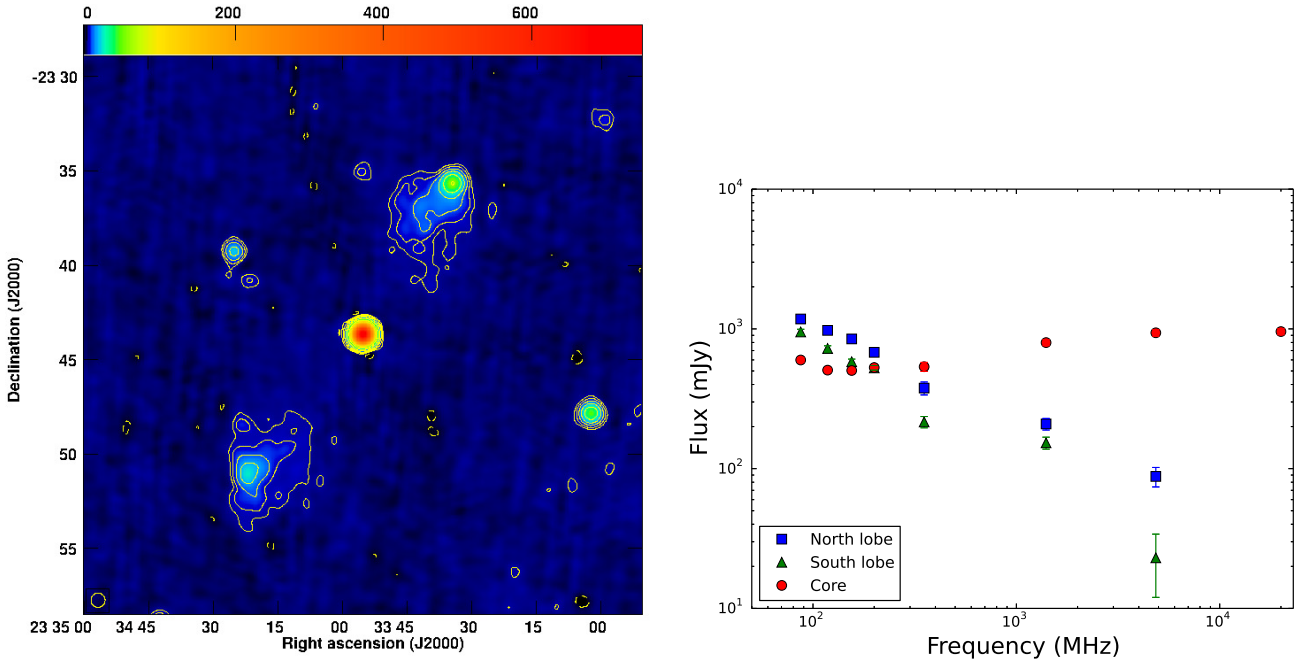

Fig. 6. *Left*: NVSS image at 1.4 GHz of the field of PBC J2333.9-2343. Contours are traced at $(-1, 1, 2, 4, 8, 16, 32) \times 1.7$ mJy beam^{-1}. The peak intensity is located at the core position and it is 747 mJy beam^{-1}. The restoring beam is circular with a 45 arcsec FWHM. *Right*: spectra of the north lobe (blue squares), core (red circles), and south lobe (green triangles). Additionally to NVSS data, we included the data up to 200 MHz from GLEAM (Hurley-Walker et al. 2017); at 352 MHz from WISH (De Breuck et al. 2002); the one at 5 GHz from the PMN survey (Griffith et al. 1994). For the core, we added data from The Australia Telescope 20 GHz (AT20G) Survey (Murphy et al. 2010).

a blazar explains well why we do not see the new lobes. Another indication in favour of this picture comes from the analysis of the radio spectra of the lobes versus that of the core. We have used data from the GLEAM (Hurley-Walker et al. 2017), WISH (De Breuck et al. 2002), NVSS (Condon et al. 1998), PMN (Griffith et al. 1994), and AT20G (Murphy et al. 2010) surveys to estimate the flux densities of the core and the lobes at different frequencies (see Fig. 6, right panel). Here it can be seen that the emission of both lobes is decaying with a steep spectrum, –0.64 for the northern lobe, and –0.86 for the southern one, whereas the emission from the core is inverted, with a spectral index of 0.15, indicative of the presence of a compact core. Although this might indicate ageing due to radiative losses in the lobes, the current data are not accurate enough to support such a claim because we cannot constrain a break at high frequencies. Notwithstanding, Giovannini et al. (2001) reported a correlation between the power of the core at 5 GHz, P_c, and the total power (lobes plus core) at 408 MHz, P_T, suggesting that sources with different kiloparsec-scale morphology and radio power are similar on parsec scales. For PBC J2333.9-2343 we estimate $\log P_T = 24.73$ from extrapolation from the emission at 352 MHz, thus from the correlation in Giovannini et al. (2001) we expect a value of $\log P_C$(theoretical) = 22.93. However, observationally we estimate a value of $\log P_c = 24.65$. This suggests either beaming, with $\theta < 20°$, or restarting activity in PBC J2333.9-2343, because the nucleus is much brighter than expected. Although we cannot differentiate between these possibilities with the current data, it is worth noting that both are in agreement with a small viewing angle for the core component, and thus with a change in the direction of the jet.

Recurrent activity is rarely seen in radio galaxies that are not giant, because the conditions inside the cocoon might favour the propagation of the lobes only after a long time from the activity burst (Marecki et al. 2006). Moreover, the selection of sources with indication of restarting activity is usually based on the radio morphology of the galaxies as DDRG or XRG (see e.g. Saikia & Jamrozy 2009). Therefore we could be missing a fraction of restarted galaxies for orientation reasons, such as the case of PBC J2333.9-2343. Indeed, it has been suggested that DDRG could be XRG with a close-to-zero misalignment. PBC J2333.9-2343 represents an extreme case of recurrent activity because all of the following situations are occurring in the same source: (i) the jet has changed its orientation; (ii) the change has occurred on the plane of the sky; (iii) the jet is now pointing towards the observer; and (iv) the jet is relatively compact and therefore young, meaning that we do not find any evidence for a diffuse morphology around the core.

Many studies have argued that the most plausible reason for the restarting activity in AGN is related to phenomenon of galaxy merging (Lara et al. 1999; Schoenmakers et al. 2000; Liu 2004; Marecki et al. 2006), because this is able to trigger the nuclear activity (e.g. Stockton & MacKenty 1983). A visual inspection of the optical images in NED[11] shows that there is a source located about 1′ from PBC J2333.9-2343 at RA = 23h33m58.8s, Dec = –23d42m54s. This galaxy has a redshift of 0.05964 as estimated by Jones et al. (2009) using an optical spectrum. Using these redshifts, we obtain that the luminosity distances are 193.3 Mpc for PBC J2333.9-2343 and 239.3 Mpc for the neighbour, with a comoving distance of approximately 35 h^{-1} Mpc (in case of a flat universe), indicating that the two objects are indeed somewhat far apart. Moreover, the difference in velocity between the two galaxies is approximately 3600 km s^{-1}, which means that it is implausible that they can be interacting. We recall that typical velocities in galaxy clusters are usually smaller than 1000 km s^{-1} (e.g. Tempel et al. 2014), although in some cases larger values have been reported, such as 1900 km s^{-1} for the AC 114 cluster (e.g., Proust et al. 2015). Furthermore,

[11] http://ned.ipac.caltech.edu/

recent works found that AGN-triggering is strongly luminosity-dependent (Treister et al. 2012). Major mergers have been shown to not be the dominant AGN-triggering process (e.g. Cisternas et al. 2011; Schawinski et al. 2012; Kocevski et al. 2012; Villforth et al. 2014, 2017), except for the most luminous AGN, which is not the case of PBC J2333.9-2343. In contrast, it has been shown that most AGN, 90%, were triggered by secular processes such as minor interactions (e.g. Treister et al. 2012). In particular for radio galaxies, modest mergers have been proposed to explain the triggering mechanism of FRII galaxies, whereas hot accretion from the intra cluster medium or the interstellar medium has been proposed to explain the triggering mechanism of FRI galaxies (Tadhunter 2016). PBC J2333.9-2343 is intermediate between the FRI and FRII classification, therefore we cannot discard any of these possibilities as the triggering mechanism.

In agreement with the merging hypothesis, in a few examples of restarting activity galaxies, indications of binary SMBHs have been found (see Gopal-Krishna et al. 2012, and references therein). Recently, this has been suggested for example for J1328+2752 by Nandi et al. (2017). In their case, the optical spectrum of the source showed that the central component has double-peaked line profiles with different emission strengths. However, the resolution of our spectra is six times lower that the one of the sloan digital sky survey (SDSS) spectra, therefore we cannot reject the possibility of unresolved double-peaked line profiles.

As mentioned above, we should also consider the possibility that the change in the direction of the jet could be related to changes or instabilities in the accretion disc. This occurrence has been formulated in terms of chaotic accretion for the SMBH feeding, which takes about 10^5 yr for the SMBH to grow (King & Nixon 2015; Schawinski et al. 2015). Although this timescale is compatible with the restarting activity timescale theoretically estimated by Reynolds & Begelman (1997), large amounts of mass would be required to change the spin axis of the SMBH and the direction of the jet (Nixon & King 2013). Although such large amounts of mass are not expected from accretion processes, we leave open this possibility as the origin of the restarted activity in PBC J2333.9-2343.

5. Conclusions

We performed a multiwavelength analysis of the nucleus of the GRG PBC J2333.9-2343 using simultaneous data at radio, optical, UV and X-ray frequencies. We find that its optical spectrum is of a type 1.9 AGN, that it is unabsorbed at X-ray frequencies, and we classify it as a blazar from the analysis of the radio data and SED fitting. We therefore propose that the source is at the present time a blazar, for which we have a direct view both to the jet and to the nucleus.

Indications of a change in the direction of the jet are observed when comparing VLBA and VLA data. This change has occurred in the plane of the sky, originating the actual morphology of the galaxy, which changed from being a radio galaxy to become a blazar. A comparison of the radio spectral indices of the lobes and the nucleus also favours this scenario, because the emission of the lobes is decaying, against the inverted spectrum of the nucleus. This is one of the few reports of episodic activity in an AGN where the source does not have a DDRG or XRG morphology but where the indications come from restarting activity arguments. Because the selection of restarting activity is usually based on radio morphologies of the sources, we notice that we might be missing a non-negligible fraction of these galaxies, meaning that the case of PBC J2333.9-2343 may not be exceptional. A comparison of the spectra of the lobes and the nuclei of a large sample of radio galaxies would be an optimal test to find more restarting activity galaxy candidates and to provide a more reliable estimate of their fraction.

A neighbour galaxy is located close to this source, but we do not see indications of recent merging events. Although we cannot rule out a possible merger, we leave open the possibility of chaotic accretion being responsible for the changes observed in this galaxy. The accretion properties and detailed analysis of the optical spectra of the source will be discussed in a forthcoming paper. The unique sensitivity and angular resolution of the Square Kilometer Array (SKA) will allow the discovery of a large number of galaxies with recurrent activity, even among the youngest and smaller systems, drawing a statistical meaningful distribution of quiescent and active phases, fundamental to constrain the physics of accretion and ejection in galaxy history.

Acknowledgements. We are especially grateful to Dr. Parisi for leading the observing proposals. Thanks to Dr. J. Masegosa, Dr. I. Márquez, Dr. C. Cicone, Dr. E. Huerta, Dr. G. Migliori, Dr. P. Gandhi, Dr. S. Lotti, Dr. F. Nicastro, Dr. I. Saviane, Dr. A. Wolter, E.F. Jiménez Andrade, Dr. C. Tadhunter, Dr. A. King, and Dr. R. Morganti for helpful and pleasant discussions during this work. We thank the anonymous referee for their comments, which helped to improve the quality of the manuscript. L.H.G. and F.P. acknowledge the ASI/INAF agreement number 2013-023-R1. MG acknowledges funding by a PRIN-INAF 2014 grant. M.P. acknowledges financial support from the Spanish Ministry of Economy and Competitiveness (MINECO) through projects AYA2013-42227-P and AYA2016-76682C3-1-P, and from the Ethiopian Space Science and Technology Institute (ESSTI) under the Ethiopian Ministry of Science and Technology (MoST). We thank the STARLIGHT team for making their code public. In this work we used IRAF, the Image Analysis and Reduction Facility made available to the astronomical community by the National Optical Astronomy Observatories, which are operated by the Association of Universities for Research in Astronomy (AURA), Inc., under contract with the US National Science Foundation. The National Radio Astronomy Observatory is a facility of the National Science Foundation operated under cooperative agreement by Associated Universities, Inc. This research made use of data obtained from the *XMM-Newton* Data Archive provided by the *XMM-Newton* Science Archive (XSA). This research made use of the NASA/IPAC extragalactic database (NED), which is operated by the Jet Propulsion Laboratory under contract with the National Aeronautics and Space Administration. This research has made use of data provided by the High Energy Astrophysics Science Archive Research Center (HEASARC), which is a service of the Astrophysics Science Division at NASA/GSFC and the High Energy Astrophysics Division of the Smithsonian Astrophysical Observatory.

References

Alexander, P., & Leahy, J. P. 1987, MNRAS, 225, 1
Andernach, H., Jiménez Andrade, E. F., & Coziol, R. 2015, in Poster presented at the international meeting "Back at the Edge of the Universe: Latest results from the deepest astronomical surveys", http://deep15.oal.ul.pt
Bahcall, J. N., Kirhakos, S., Saxe, D. H., & Schneider, D. P. 1997, ApJ, 479, 642
Baldwin, J. A., Wampler, E. J., & Burbidge, E. M. 1981, ApJ, 243, 76
Bassani, L., Dadina, M., Maiolino, R., et al. 1999, ApJS, 121, 473
Bassani, L., Venturi, T., Molina, M., et al. 2016, MNRAS, 461, 3165
Bruzual, G., & Charlot, S. 2003, MNRAS, 344, 1000
Burtscher, L., Davies, R. I., Graciá-Carpio, J., et al. 2016, A&A, 586, A28
Cardelli, J. A., Clayton, G. C., & Mathis, J. S. 1989, ApJ, 345, 245
Christiansen, W. A. 1973, MNRAS, 164, 211
Cid Fernandes, R., Mateus, A., Sodré, L., Stasińska, G., & Gomes, J. M. 2005, MNRAS, 358, 363
Cid Fernandes, R., Schoenell, W., Gomes, J. M., et al. 2009, Rev. Mex. Astron. Astrofis. Conf. Ser., 35, 127
Cisternas, M., Jahnke, K., Inskip, K. J., et al. 2011, ApJ, 726, 57
Condon, J. J., Cotton, W. D., Greisen, E. W., et al. 1998, AJ, 115, 1693
D'Abrusco, R., Massaro, F., Paggi, A., et al. 2014, ApJS, 215, 14
De Breuck, C., Tang, Y., de Bruyn, A. G., Röttgering, H., & van Breugel, W. 2002, A&A, 394, 59
Dennett-Thorpe, J., Scheuer, P. A. G., Laing, R. A., et al. 2002, MNRAS, 330, 609
Dickey, J. M., & Lockman, F. J. 1990, ARA&A, 28, 215

Evans, A. S., Sanders, D. B., Surace, J. A., & Mazzarella, J. M. 1999, ApJ, 511, 730
Fomalont, E. B., Frey, S., Paragi, Z., et al. 2000, ApJS, 131, 95
Ghisellini, G., & Tavecchio, F. 2009, MNRAS, 397, 985
Ghisellini, G., & Tavecchio, F. 2015, MNRAS, 448, 1060
Giommi, P., Polenta, G., Lähteenmäki, A., et al. 2012, A&A, 541, A160
Giovannini, G., Cotton, W. D., Feretti, L., Lara, L., & Venturi, T. 2001, ApJ, 552, 508
Giovannini, G., Taylor, G. B., Feretti, L., et al. 2005, ApJ, 618, 635
Giovannini, G., Giroletti, M., & Taylor, G. B. 2007, A&A, 474, 409
González-Martín, O., & Vaughan, S. 2012, A&A, 544, A80
Gopal-Krishna, Biermann, P. L., Gergely, L. Á., & Wiita, P. J. 2012, RA&A, 12, 127
Graham, P. J., & Tingay, S. J. 2014, ApJ, 784, 159
Greene, J. E., & Ho, L. C. 2005, ApJ, 630, 122
Griffith, M. R., Wright, A. E., Burke, B. F., & Ekers, R. D. 1994, ApJS, 90, 179
Gültekin, K., Richstone, D. O., Gebhardt, K., et al. 2009, ApJ, 698, 198
Hatziminaoglou, E., Siemiginowska, A., & Elvis, M. 2001, ApJ, 547, 90
Healey, S. E., Romani, R. W., Taylor, G. B., et al. 2007, ApJS, 171, 61
Hernández-García, L., González-Martín, O., Márquez, I., & Masegosa, J. 2013, A&A, 556, A47
Hurley-Walker, N., Callingham, J. R., Hancock, P. J., et al. 2017, MNRAS, 464, 1146
Ishwara-Chandra, C. H., & Saikia, D. J. 1999, MNRAS, 309, 100
Jones, D. H., Read, M. A., Saunders, W., et al. 2009, MNRAS, 399, 683
Kalberla, P. M. W., Burton, W. B., Hartmann, D., et al. 2005, A&A, 440, 775
Kellermann, K. I., Sramek, R., Schmidt, M., Shaffer, D. B., & Green, R. 1989, AJ, 98, 1195
King, A., & Nixon, C. 2015, MNRAS, 453, L46
Kocevski, D. D., Faber, S. M., Mozena, M., et al. 2012, ApJ, 744, 148
Konar, C., Saikia, D. J., Jamrozy, M., & Machalski, J. 2006, MNRAS, 372, 693
Konar, C., Jamrozy, M., Saikia, D. J., & Machalski, J. 2008, MNRAS, 383, 525
Kormendy, J., & Richstone, D. 1995, ARA&A, 33, 581
Kraft, R. P., Hardcastle, M. J., Worrall, D. M., & Murray, S. S. 2005, ApJ, 622, 149
Lal, D. V., & Rao, A. P. 2007, MNRAS, 374, 1085
Lara, L., Márquez, I., Cotton, W. D., et al. 1999, A&A, 348, 699
Leahy, J. P., & Williams, A. G. 1984, MNRAS, 210, 929
Liu, F. K. 2004, MNRAS, 347, 1357
Liu, R., Pooley, G., & Riley, J. M. 1992, MNRAS, 257, 545
Machalski, J., Kozieł-Wierzbowska, D., Jamrozy, M., & Saikia, D. J. 2008, ApJ, 679, 149
Maiolino, R., Salvati, M., Bassani, L., et al. 1998, A&A, 338, 781
Marecki, A. 2012, A&A, 544, L2
Marecki, A., Thomasson, P., Mack, K.-H., & Kunert-Bajraszewska, M. 2006, A&A, 448, 479
Mason, K. O., Breeveld, A., Much, R., et al. 2001, A&A, 365, L36
Massaro, E., Giommi, P., Leto, C., et al. 2009, A&A, 495, 691
Massey, P., Strobel, K., Barnes, J. V., & Anderson, E. 1988, ApJ, 328, 315
Merritt, D., & Ekers, R. D. 2002, Science, 297, 1310
Murphy, T., Sadler, E. M., Ekers, R. D., et al. 2010, MNRAS, 402, 2403
Nagai, H., Chida, H., Kino, M., et al. 2016, Astron. Nachr., 337, 69
Nandi, S., Jamrozy, M., Roy, R., et al. 2017, MNRAS, 467, L56
Narayan, R., & Yi, I. 1994, ApJ, 428, L13
Nixon, C., & King, A. 2013, ApJ, 765, L7
Ojha, R., Fey, A. L., Johnston, K. J., et al. 2004, AJ, 127, 3609
Osterbrock, D. E. 1981, ApJ, 249, 462
Panessa, F., Bassani, L., Landi, R., et al. 2016, MNRAS, 461, 3153
Parisi, P., Masetti, N., Jiménez-Bailón, E., et al. 2012, A&A, 545, A101
Pović, M., Márquez, I., Netzer, H., et al. 2016, MNRAS, 462, 2878
Proust, D., Yegorova, I., Saviane, I., et al. 2015, MNRAS, 452, 3304
Rees, M. J. 1978, Nature, 275, 516
Rees, M. J. 1984, ARA&A, 22, 471
Reynolds, C. S., & Begelman, M. C. 1997, ApJ, 487, L135
Ricci, R., Prandoni, I., Gruppioni, C., Sault, R. J., & De Zotti, G. 2004, A&A, 415, 549
Risaliti, G., Bassani, L., Comastri, A., et al. 1999, Mem. Soc. Astron. Ital., 70, 73
Rottmann, H. 2001, Ph.D. Thesis, Bonn, Germany
Saikia, D. J., & Jamrozy, M. 2009, BASI, 37, 63
Saikia, D. J., Jamrozy, M., Konar, C., & Nandi, S. 2010, in 25th Texas Symp. on Relativistic Astrophysics, 14
Salpeter, E. E. 1964, ApJ, 140, 796
Saripalli, L., Subrahmanyan, R., & Udaya Shankar, N. 2002, ApJ, 565, 256
Saripalli, L., Malarecki, J. M., Subrahmanyan, R., Jones, D. H., & Staveley-Smith, L. 2013, MNRAS, 436, 690
Schawinski, K., Simmons, B. D., Urry, C. M., Treister, E., & Glikman, E. 2012, MNRAS, 425, L61
Schawinski, K., Koss, M., Berney, S., & Sartori, L. F. 2015, MNRAS, 451, 2517
Schoenmakers, A. P., Mack, K.-H., Lara, L., et al. 1998, A&A, 336, 455
Schoenmakers, A. P., de Bruyn, A. G., Röttgering, H. J. A., van der Laan, H., & Kaiser, C. R. 2000, MNRAS, 315, 371
Shakura, N. I., & Sunyaev, R. A. 1973, A&A, 24, 337
Stockton, A., & MacKenty, J. W. 1983, Nature, 305, 678
Strüder, L., Briel, U., Dennerl, K., et al. 2001, A&A, 365, L18
Tadhunter, C. 2016, A&ARv, 24, 10
Tempel, E., Tamm, A., Gramann, M., et al. 2014, A&A, 566, A1
Treister, E., Schawinski, K., Urry, C. M., & Simmons, B. D. 2012, ApJ, 758, L39
Vaughan, S., Edelson, R., Warwick, R. S., & Uttley, P. 2003, MNRAS, 345, 1271
Venturi, T., Dallacasa, D., & Stefanachi, F. 2004, A&A, 422, 515
Villforth, C., Hamann, F., Rosario, D. J., et al. 2014, MNRAS, 439, 3342
Villforth, C., Hamilton, T., Pawlik, M. M., et al. 2017, MNRAS, 466, 812
Walker, R. 2015, Flux Density Calibration on the VLBA, Tech. Rep., http://library.nrao.edu/public/memos/vlba/sci/VLBAS_37.pdf
Wilkes, B. J., Wright, A. E., Jauncey, D. L., & Peterson, B. A. 1983, PASA, 5, 2